PERGAMON

International Journal of Solids and Structures 36 (1999) 4473–4496

INTERNATIONAL JOURNAL OF SOLIDS and STRUCTURES

Spherically isotropic, elastic spheres subject to diametral point load strength test

K. T. Chau*, X. X. Wei

Department of Civil and Structural Engineering, The Hong Kong Polytechnic University, Kowloon, Hong Kong, China

Received 4 January 1998; in revised form 17 June 1998

Abstract

This paper presents an analytic solution for the stress concentrations within a spherically isotropic, elastic sphere of radius R subject to diametral point load strength test. The method of solution uses the displacement potential approach together with the Fourier–Legendre expansion for the boundary loads. For the case of isotropic sphere, our solution reduces to the solution by Hiramatsu and Oka (1966) and agrees well with the published experimental observations by Frocht and Guernsey (1953). A zone of higher tensile stress concentration is developed near the point loads, and the difference between this maximum tensile stress and the uniform tensile stress in the central part of the sphere increases with E/E' (where E and E' are the Young's moduli governing axial deformations along directions parallel and normal to the planes of isotropy, respectively), G'/G (where G and G' are the moduli governing shear deformations in the planes of isotropy and the planes parallel to the radial direction), and $\bar{\nu}/\nu'$ (where $\bar{\nu}$ and ν' are the Poisson's ratios characterizing transverse reduction in the planes of isotropy under tension in the same plane and under radial tension, respectively). This stress difference, in general, decreases with the size of loading area and the Poisson's ratio.

Keywords: Point load strength test; Spherically isotropic; Spheres; Stress analysis; Displacement functions

1. Introduction

Point Load Strength Test (PLST) is a convenient and inexpensive method for rock classification and rock strength estimation (e.g. Broch and Franklin, 1972; Guidicini et al., 1973; Bieniawski, 1974). The required apparatus for PLST is light and portable (Boisen, 1977). The point load strength test can be applied to rock cores (either axially or diametrically), to spheres, or to irregular lumps as shown in Fig. 1. The testing procedure has been standardized by the International Society for Rock Mechanics (ISRM, 1985). In addition to rock testing, PLST has also be applied to estimate both tensile and compressive strengths of concrete (Robins, 1980; Richardson, 1989) and reinforced concrete (Robins and Austin, 1985).

* Corresponding author. Tel.: 00852 23346389; Fax: 00852 2666015; E-mail: cektchau@polyu.edu.hk

0020-7683/99/$ - see front matter
PII: S0020-7683(98)00202-9

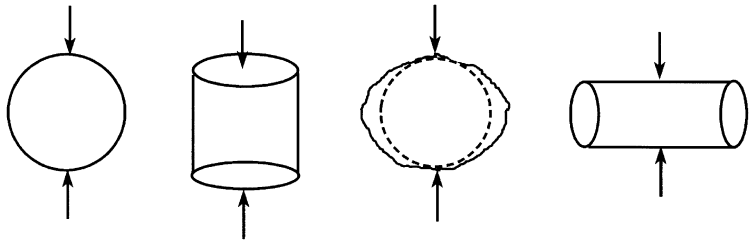

Fig. 1. Test specimens used for PLST (from the left): sphere, cylinder under axial point loads, irregular lump, cylinder under diametral point loads.

Extensive experimental studies have been done on PLST (see the review by Chau and Wong, 1996), but there are relatively few theoretical studies for PLST. Analytical studies for PLST include the analyses of isotropic spheres subject to a pair of diametrical point loads by Hiramatsu and Oka (1966), finite cylinders subject to axial point loads by Wijk (1978) and Chau and Wong (1996), and finite cylinders subject to diametral point loads by Wijk (1980) and Chau (1998a).

All of these analyses are restricted to isotropic solids, there is no analytic solution for the PLST for anisotropic solids. However, in reality most of the natural rocks, are, to certain extent, anisotropic in nature. PLST has also been commonly applied in testing the strength of anisotropic rocks (e.g. Hassani et al., 1980; Lajtai, 1980; Read et al. 1980; Greminger, 1982; Forster, 1983; Broch, 1983).

Therefore, in this paper we investigate the effect of material anisotropy on the tensile stress concentration within rock specimens subject to PLST by considering the simplest problem: a spherically isotropic elastic sphere subject to the diametral PLST. The solution to be presented here can be considered as an extension of the classical solution for isotropic spheres obtained by Hiramatsu and Oka (1966). Spherically isotropic solid, which was first introduced by Saint-Venant in 1865 (see the historical account by Love, 1944), is the simplest type of anisotropic solids and contains five independent material constants. The diametral point loads are modeled by a uniform distribution of radial stress applied on two finite regions of the spherical surface, which is further expanded in Fourier–Legendre series as proposed by Hiramatsu and Oka (1966).

Although most of the rock specimens available for PLST are either cylindrical (i.e. rock cores) or irregular (i.e. rock lumps), solution of the tensile stress concentration in spheres under diametral point loads has been found very meaningful for the PLSTs. It provides not only a theoretical basis for the testing of irregular lumps of rocks (Hiramatsu and Oka, 1966), but also an upper bound of the tensile stress concentration within a cylindrical specimen under the diametral point load test (e.g. see Wijk, 1980). More specifically, Wijk (1980) obtained an approximation for the tensile stress concentration at the center of a cylinder under diametral point loads, which is found intermediate between the solutions of the same problem for a circular plate and for a sphere. Then, the tensile stress distribution along the diameter of a cylinder under diametral PLST can be approximated by interpolating the solutions for circular pates given by Wijk (1978) and for spheres given by Hiramatsu and Oka (1966) (see for example Fig. 2 of Wijk, 1980). Therefore, the solution for spheres does shed light on the stress analysis of the diametral PLST for cylindrical rock cores.

The compression of isotropic spheres by either force or displacement control is one of the most fundamental problems in the mathematical theory of elasticity and has been considered by various authors. Sternberg and Rosenthal (1952) first solved the problems of isotropic spheres under concentrated diametral loads by using the Boussinesq stress-function in dipolar coordinates, and their solutions have been verified by comparison to the experiments by Frocht and Guernsey (1953). When the diametral point loads are distributed over two finite areas on the spherical surface, the problem was solved by Hiramatsu and Oka (1966), and the analysis was motivated by the PLST for irregular lumps. Experimental and stress analyses for large deformations of spheres compressed between two rigid blocks have been done by Frocht and Guernsey (1953), Durelli and Daniel (1961), Durelli and Chen (1973), and Chen and Durelli (1973), Tatara (1991) and Tatara et al. (1991). When the loads are transferred to the elastic spheres through displacement boundary conditions, the problem was analyzed by Abramian et al. (1964). However, all of these analyses are restricted to isotropic spheres, no stress analysis has been done on anisotropic spheres under diametral point loads.

Actually, except the theoretical analyses by Nowinski (1959), Eason (1962), Chen (1966), Hata (1993), Ding and Ren (1991) and Chau (1995, 1998b) for spherically isotropic spheres, not many analytical solutions exist for spherically isotropic materials or spheres.

The method of solutions used here follows the general theory for spherically isotropic solids proposed recently by Ding and Ren (1991), which is modified from the general theory by Hu (1954). In particular, the displacement functions proposed by Hu (1954) will be applied to the equations of equilibrium, then a change of variables proposed by Ding and Ren (1991) is used such that closed-form solutions for the roots of the characteristic equation of the governing equations can be found. Displacement functions are expressed in terms of spherical harmonics, and in turn all stress components can also be expressed in terms of spherical harmonics. To obtain the final solutions, applied loads on the spherical surface are expanded in terms of Fourier–Legendre series (as employed by Hiramatsu and Oka, 1966) and match with the boundary values of the normal stresses of the spheres. Finally, a closed form solution can be obtained for the stress concentration. As expected, the isotropic limit of our solution recovers the classical solution by Hiramatsu and Oka (1966), and compares well with the experimental observations obtained by Frocht and Guernsey (1953) using the method of photoelasticity.

In real PLST, the diametral point loads are applied to the rock specimens through steel cones with spherical heads (e.g. ISRM, 1985). Therefore, the actual boundary conditions of the applied loads should more realistically be modeled by contact between the spherical rock and the steel cone, as proposed by Chau (1998a). It is also relevant to mention here that the contact problem between two identical transversely isotropic spheres has been solved by Keer and Mowry (1979). However, in order to recover the classical solution by Hiramatsu and Oka (1966) and to avoid more tedious calculations, we, by following Hiramatsu and Oka (1966), model the applied load by assuming a uniform normal stress applied over two opposite finite patches on the sphere. The actual contact problem between the steel cones and the anisotropic rock specimen and the study on inelastic crushing of the rock at the contact are complicated problems and out of the scope of the present study. We refer to Zhang et al. (1990) and Shah and Wong (1996, 1997) for some recent developments. The main focus here will be on the effect of material anisotropy on the tensile stress concentration within the spherical rock specimen.

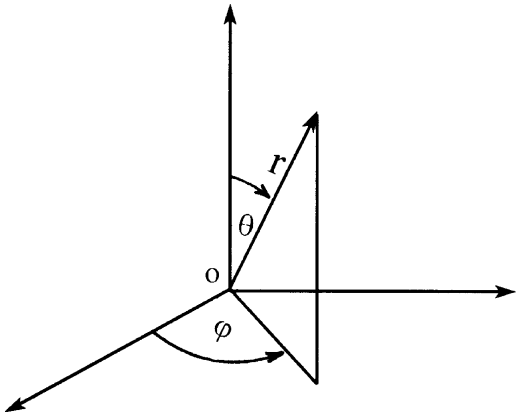

Fig. 2. The spherical polar coordinate system used.

2. Governing equations

2.1. Hooke's law

Consider a spherical polar coordinate system (r, θ, φ) with the origin locating at the center of the sphere, as shown in Fig. 2. The spherical rock specimen is assumed to be linear elastic and spherically isotropic, and the stress and strain components are related by the following generalized Hooke's law

$$\varepsilon_{\theta\theta} = \frac{\sigma_{\theta\theta}}{E} - \frac{\bar{\nu}\sigma_{\varphi\varphi}}{E} - \frac{\nu'\sigma_{rr}}{E'}, \quad \varepsilon_{\varphi\varphi} = -\frac{\bar{\nu}\sigma_{\theta\theta}}{E} + \frac{\sigma_{\varphi\varphi}}{E} - \frac{\nu'\sigma_{rr}}{E'}$$

$$\varepsilon_{rr} = -\frac{\nu'}{E'}(\sigma_{\theta\theta} + \sigma_{\varphi\varphi}) + \frac{\sigma_{rr}}{E'}, \quad \varepsilon_{\theta\varphi} = \frac{(1+\bar{\nu})}{E}\sigma_{\theta\varphi}, \quad \varepsilon_{r\alpha} = \frac{\sigma_{r\alpha}}{2G'} \tag{1}$$

where $\alpha = \theta, \varphi$. The Cauchy stress tensor is denoted by σ and the strain tensor by ε. Physically, E and E' are the Young's moduli governing axial deformations on the planes of isotropy (i.e. any tangential plane on a spherical surface drawn from the origin) and along direction perpendicular to it (i.e. the radial direction), respectively. The Poisson's ratios $\bar{\nu}$ and ν' characterize transverse reduction in the planes of isotropy under tension in the same plane and under radial tension, respectively. The shear modulus G' governs the shear deformation of on the planes with unit normals perpendicular to the radial direction.

In order to make our Hooke's law compatible to others (e.g. Hu, 1954; Ding and Ren, 1991), (1) is inverted to give

$$\sigma_{\theta\theta} = (2A_{66} + A_{12})\varepsilon_{\theta\theta} + A_{12}\varepsilon_{\varphi\varphi} + A_{13}\varepsilon_{rr}$$

$$\sigma_{\varphi\varphi} = A_{12}\varepsilon_{\theta\theta} + (2A_{66} + A_{12})\varepsilon_{\varphi\varphi} + A_{13}\varepsilon_{rr}$$

$$\sigma_{rr} = A_{13}(\varepsilon_{\theta\theta} + \varepsilon_{\varphi\varphi}) + A_{33}\varepsilon_{rr}, \quad \sigma_{\theta\varphi} = 2A_{66}\varepsilon_{\theta\varphi}, \quad \sigma_{r\alpha} = 2A_{44}\varepsilon_{r\alpha} \tag{2}$$

where

$$A_{12} = -\frac{E(\bar{\nu}E' + \nu'^2 E)}{(1+\bar{\nu})\bar{E}}, \quad A_{13} = -\frac{\nu' E' E}{\bar{E}}, \quad A_{33} = -\frac{E'^2(1-\bar{\nu})}{\bar{E}}$$

$$A_{66} = \frac{E}{2(1+\bar{\nu})}, \quad A_{44} = G', \quad \bar{E} = E'(\bar{\nu}-1) + 2\nu'^2 E \tag{3}$$

For small deformation and small strain, the relations between the strain and displacement components in spherical polar coordinate are expressed as

$$\varepsilon_{rr} = \frac{\partial u_r}{\partial r}, \quad \varepsilon_{\theta\theta} = \frac{1}{r}\frac{\partial u_\theta}{\partial \theta} + \frac{u_r}{r}, \quad \varepsilon_{\varphi\varphi} = \frac{1}{r\sin\theta}\frac{\partial u_\varphi}{\partial \varphi} + \frac{u_r}{r} + \frac{u_\theta}{r}\cot\theta$$

$$\varepsilon_{r\varphi} = \frac{1}{2}\left(\frac{1}{r\sin\theta}\frac{\partial u_r}{\partial \varphi} - \frac{u_\varphi}{r} + \frac{\partial u_\varphi}{\partial r}\right), \quad \varepsilon_{r\theta} = \frac{1}{2}\left(\frac{1}{r}\frac{\partial u_r}{\partial \theta} - \frac{u_\theta}{r} + \frac{\partial u_\theta}{\partial r}\right)$$

$$\varepsilon_{\theta\varphi} = \frac{1}{2}\left(\frac{1}{r}\frac{\partial u_\varphi}{\partial \theta} - \frac{u_\varphi}{r}\cot\theta + \frac{1}{r\sin\theta}\frac{\partial u_\theta}{\partial \varphi}\right) \tag{4}$$

where u_θ, u_φ and u_r are displacements in θ, φ and r directions, respectively.

2.2. Equilibrium equations

For the present problem of spheres under diametral compression, body forces can be neglected. Hence, the equations of equilibrium can be simplified to

$$\frac{\partial \sigma_{rr}}{\partial r} + \frac{1}{r\sin\theta}\frac{\partial \sigma_{r\varphi}}{\partial \varphi} + \frac{1}{r}\frac{\partial \sigma_{r\theta}}{\partial \theta} + \frac{2\sigma_{rr} - \sigma_{\theta\theta} - \sigma_{\varphi\varphi} + \sigma_{r\theta}\cot\theta}{r} = 0$$

$$\frac{\partial \sigma_{r\varphi}}{\partial r} + \frac{1}{r\sin\theta}\frac{\partial \sigma_{\varphi\varphi}}{\partial \varphi} + \frac{1}{r}\frac{\partial \sigma_{\theta\varphi}}{\partial \theta} + \frac{3\sigma_{r\varphi} + 2\sigma_{\theta\varphi}\cot\theta}{r} = 0$$

$$\frac{\partial \sigma_{r\theta}}{\partial r} + \frac{1}{r\sin\theta}\frac{\partial \sigma_{\theta\varphi}}{\partial \varphi} + \frac{1}{r}\frac{\partial \sigma_{\theta\theta}}{\partial \theta} + \frac{3\sigma_{r\theta} + (\sigma_{\theta\theta} - \sigma_{\varphi\varphi})\cot\theta}{r} = 0 \tag{5}$$

Substituting (2) and (4) into (5), we obtain

$$-2(A_{12}+A_{66})\frac{\varepsilon}{r} + A_{13}\left(\frac{\partial \varepsilon}{\partial r} + \frac{2\varepsilon}{r} - \frac{2\varepsilon_{rr}}{r}\right) + A_{33}\left(\frac{\partial \varepsilon_{rr}}{\partial r} + \frac{2\varepsilon_{rr}}{r}\right) + A_{44}\left[\frac{1}{r^2}\nabla_1^2 u_r + \frac{\partial}{\partial r}\left(\varepsilon - \frac{2u_r}{r}\right)\right] = 0$$

$$\frac{A_{12}}{r\sin\theta}\frac{\partial \varepsilon}{\partial \varphi} + 2A_{66}\left(\frac{1}{r\sin\theta}\frac{\partial \varepsilon_{\varphi\varphi}}{\partial \varphi} + \frac{1}{r}\frac{\partial \varepsilon_{\theta\varphi}}{\partial \theta} + \frac{2\cot\theta}{r}\varepsilon_{\theta\varphi}\right) + \frac{A_{13}}{r\sin\theta}\frac{\partial \varepsilon_{rr}}{\partial \varphi} + 2A_{44}\left(\frac{\partial \varepsilon_{r\varphi}}{\partial r} + \frac{3\varepsilon_{r\varphi}}{r}\right) = 0$$

$$\frac{A_{12}}{r}\frac{\partial \varepsilon}{\partial \theta} + 2A_{66}\left[\frac{1}{r\sin\theta}\frac{\partial \varepsilon_{\theta\varphi}}{\partial \varphi} + \frac{1}{r}\frac{\partial \varepsilon_{\theta\theta}}{\partial \theta} + \frac{\cot\theta}{r}(\varepsilon_{\theta\theta} - \varepsilon_{\varphi\varphi})\right] + \frac{A_{13}}{r}\frac{\partial \varepsilon_{rr}}{\partial \theta} + 2A_{44}\left(\frac{\partial \varepsilon_{r\theta}}{\partial r} + \frac{3\varepsilon_{r\theta}}{r}\right) = 0 \tag{6}$$

where

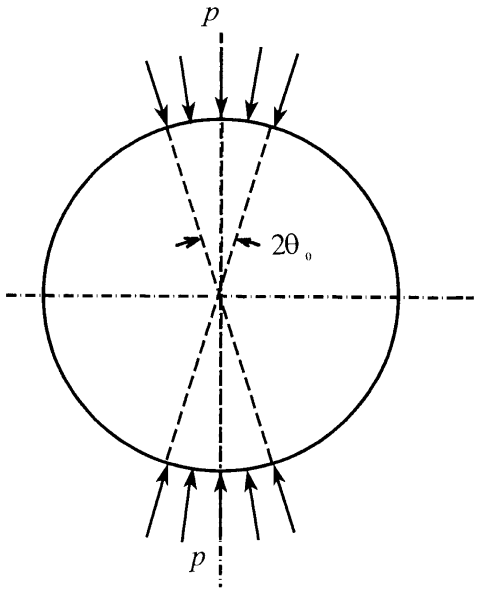

Fig. 3. A sphere under PLST is modeled by uniform radial stress applied over two small spherical areas subtending an angle of $2\theta_0$.

$$\varepsilon = \varepsilon_{\theta\theta} + \varepsilon_{\varphi\varphi} \tag{7}$$

$$\nabla_1^2 = \frac{\partial^2}{\partial\theta^2} + \cot\theta\frac{\partial}{\partial\theta} + \frac{1}{\sin^2\theta}\frac{\partial^2}{\partial\varphi^2} \tag{8}$$

2.3. Boundary conditions

For the diametral compression of spheres of radius R, the pair of point forces of magnitude F are modeled by uniform radial stress p applied over two opposite spherical areas (on $r = R$) which subtend an angle of $2\theta_0$ from the origin symmetrically with respect to the z-axis, as shown in Fig. 3. All other tractions are zero on $r = R$. Mathematically, this boundary condition can be expressed as:

$$\sigma_{rr} = \begin{cases} -p & \text{for } 0 \leqslant \theta \leqslant \theta_0 \quad \text{and} \quad \pi - \theta_0 \leqslant \theta \leqslant \pi \\ 0 & \text{for } \theta_0 < \theta < \pi - \theta_0 \end{cases} \tag{9}$$

$$\sigma_{r\varphi} = \sigma_{r\theta} = 0 \tag{10}$$

on $r = R$, where p can be expressed in terms of F, R and θ_0 as (Hiramatsu and Oka, 1966):

$$p = F/[2\pi R^2(1-\cos\theta_0)] \tag{11}$$

Now, our problem is to solve the equilibrium eqns (6) subject to boundary conditions (9) and (10). The technique of displacement function and the method of solutions are considered next.

3. Displacement functions

It was proposed by Hu (1954) that the displacements under consideration can be resolved into two parts: the first displacement field corresponds to both the radial displacement and the dilatation equal to zero; and the second field corresponds to the radial component of the curl of the displacements equal to zero. More specifically, the displacements are decomposed into (Hu, 1954):

$$\begin{aligned} u_r &= u_r^{\mathrm{I}} + u_r^{\mathrm{II}} = 0 + w \\ u_\theta &= u_\theta^{\mathrm{I}} + u_\theta^{\mathrm{II}} = -\frac{1}{r\sin\theta}\frac{\partial\psi}{\partial\varphi} - \frac{1}{r}\frac{\partial G}{\partial\theta} \\ u_\varphi &= u_\varphi^{\mathrm{I}} + u_\varphi^{\mathrm{II}} = \frac{1}{r}\frac{\partial\psi}{\partial\theta} - \frac{1}{r\sin\theta}\frac{\partial G}{\partial\varphi} \end{aligned} \tag{12}$$

where ψ and G are displacement functions. Substitution of (12) into (6) leads to the following partial differential equations

$$\frac{2(a+b)}{r^3}\nabla_1^2 G - \frac{d}{r^2}\nabla_1^2\frac{\partial G}{\partial r} + \frac{2g}{r^2}w + \frac{c}{r^2}\frac{\partial}{\partial r}\left(r^2\frac{\partial w}{\partial r}\right) + \frac{h}{r^2}\nabla_1^2 w = 0 \tag{13}$$

$$\frac{1}{r}\frac{\partial B}{\partial\theta} + \frac{1}{r\sin\theta}\frac{\partial A}{\partial\varphi} = 0 \tag{14}$$

$$\frac{1}{r}\frac{\partial A}{\partial\theta} - \frac{1}{r\sin\theta}\frac{\partial B}{\partial\varphi} = 0 \tag{15}$$

in which A and B are functions expressed in terms of w, G, and ψ

$$A = -\frac{a}{r^2}\nabla_1^2 G + \frac{2b}{r^2}G - h\frac{\partial^2 G}{\partial r^2} + \frac{2(a+b)}{r}w + d\frac{\partial w}{\partial r} \tag{16}$$

$$B = (h-b)\left(\frac{1}{r^2}\nabla_1^2\psi + \frac{2\psi}{r^2}\right) + h\left(\frac{\partial^2\psi}{\partial r^2} - \frac{2\psi}{r^2}\right) \tag{17}$$

$$\begin{aligned} &a = A_{12} + 2A_{66}, \quad b = A_{44} - A_{66}, \quad d = A_{13} + A_{44} \\ &c = A_{33}, \quad h = A_{44}, \quad g = d + h - 2(a+b) \end{aligned} \tag{18}$$

As shown in Section V of Hu (1954), without loss of generality, both A and B can be set to zero; that is,

$$A = B = 0 \tag{19}$$

The proof of this result is outlined briefly in the Appendix. In order to obtain a more tractable form of the solution for (13) and (19), the following change of variables similar to those proposed by Ding and Ren (1991) is introduced

$$r = R\exp(\eta), \quad \psi = RZ\exp(\eta), \quad G = RF\exp(\eta), \quad w = -r\frac{\partial H}{\partial r} = -\frac{\partial H}{\partial\eta} \tag{20}$$

where Z, F, and H are new displacement functions in terms of the new dimensionless radial variable η, and R is the radius of the sphere. When $R = 1$, the change of variables introduced in (20) reduces to those of Ding and Ren (1991), but with the introduction of R into (20) no ambiguity in dimension will be resulted, as compared to the analysis by Ding and Ren (1991). The main reason for introducing the change of variables in (20) is that, as it will be shown later in this paper, the roots for the characteristic equation for the governing equations can be obtained explicitly, as compared to the implicit form given in eqn (33) of Hu (1954).

Substitution of (20) into (16), (17), (19) and (13) leads to the following three partial differential equations for Z, F, and H:

$$A_{44}\left(\frac{\partial^2 Z}{\partial \eta^2}+\frac{\partial Z}{\partial \eta}\right)+A_{66}\nabla_1^2 Z-2(A_{44}-A_{66})Z=0 \tag{21}$$

$$\left[h\left(\frac{\partial^2}{\partial \eta^2}+\frac{\partial}{\partial \eta}\right)+a\nabla_1^2-2b\right]F+\left[d\frac{\partial^2}{\partial \eta^2}+2(a+b)\frac{\partial}{\partial \eta}\right]H=0 \tag{22}$$

$$\left[(h-g)\nabla_1^2-d\nabla_1^2\frac{\partial}{\partial \eta}\right]F-\left[c\left(\frac{\partial^3}{\partial \eta^3}+\frac{\partial^2}{\partial \eta^2}\right)+h\nabla_1^2\frac{\partial}{\partial \eta}+2g\frac{\partial}{\partial \eta}\right]H=0 \tag{23}$$

To uncouple the governing equations for F and H, (22) and (23), another new displacement function ϕ is introduced such that

$$F=\left[d\frac{\partial^2}{\partial \eta^2}+2(a+b)\frac{\partial}{\partial \eta}\right]\phi \tag{24}$$

$$H=-\left[h\left(\frac{\partial^2}{\partial \eta^2}+\frac{\partial}{\partial \eta}\right)+a\nabla_1^2-2b\right]\phi \tag{25}$$

Then, (22) is satisfied identically by (24) and (25). Substitution of (24) and (25) into (23) yields a single governing equation for ϕ, which can be further simplified to the following form if another new potential Φ is introduced

$$\left\{\left(\frac{\partial^2}{\partial \eta^2}+\frac{\partial}{\partial \eta}\right)^2+2D\left(\frac{\partial^2}{\partial \eta^2}+\frac{\partial}{\partial \eta}\right)+M\nabla_1^2\left(\frac{\partial^2}{\partial \eta^2}+\frac{\partial}{\partial \eta}\right)-4L+2(N-L)\nabla_1^2+N\nabla_1^2\nabla_1^2\right\}\Phi=0 \tag{26}$$

where

$$D=\frac{hg-bc}{ch},\quad L=\frac{bg}{ch},\quad M=\frac{ac+h^2-d^2}{ch},\quad N=\frac{a}{c} \tag{27}$$

and Φ is defined as

$$\Phi=-\frac{\partial \phi}{\partial \eta} \tag{28}$$

Subsequently, only two displacement potentials Z and Φ remain and satisfy (21) and (26), respectively. Expressed in terms of these displacement functions, the displacement components become

$$u_\theta = -\frac{1}{\sin\theta}\frac{\partial Z}{\partial \varphi} + \left[d\frac{\partial}{\partial \eta} + 2(a+b)\right]\frac{\partial \Phi}{\partial \theta}, \quad u_\varphi = \frac{\partial Z}{\partial \theta} + \frac{1}{\sin\theta}\left[d\frac{\partial}{\partial \eta} + 2(a+b)\right]\frac{\partial \Phi}{\partial \varphi}$$

$$u_r = -\left[h\left(\frac{\partial^2}{\partial \eta^2} + \frac{\partial}{\partial \eta}\right) + a\nabla_1^2 - 2b\right]\Phi \tag{29}$$

Substitution of (29) into (4) and (2) yields the strain and stress components in terms of Z and Φ. The attractive feature of this displacement function approach is that our governing equations are reduced to two uncoupled partial differential equations, which are much easier to solve than coupled partial differential equations. But, as a tradeoff the governing equation (26) is of order higher than that of the equations of equilibrium. The general solutions for Z and Φ are discussed next.

4. General solutions for the displacement functions

Motivated by the stress analysis for isotropic spheres, the following solution form in terms of spherical harmonics is sought for the displacement function Z

$$Z = \sum_{n=0}^{\infty} D_n \, e^{\lambda_n \eta} S_n(\theta, \varphi) \tag{30}$$

where D_n and λ_n are unknown constants to be determined and $S_n(\theta, \varphi)$ is the spherical harmonics of order n, which satisfies

$$\nabla_1^2 S_n(\theta, \varphi) + n(n+1) S_n(\theta, \varphi) = 0 \tag{31}$$

Substitution of (30) into (21) leads to the following characteristic equation for λ_n

$$\lambda_n^2 + \lambda_n - M_n = 0 \tag{32}$$

where

$$M_n = 2 + (n-1)(n+2)A_{66}/A_{44} \tag{33}$$

The two characteristic roots of (32) are

$$\lambda_{n1} = \frac{-1+\sqrt{1+4M_n}}{2}, \quad \lambda_{n2} = \frac{-1-\sqrt{1+4M_n}}{2} \tag{34}$$

Consequently, if $\lambda_{n1} \neq \lambda_{n2}$, the displacement function Z defined in (29) becomes

$$Z = \sum_{n=0}^{\infty} (D_{n1} \, e^{\lambda_{n1}\eta} + D_{n2} \, e^{\lambda_{n2}\eta}) S_n(\theta, \varphi) \tag{35}$$

where D_{n1} and D_{n2} are unknown constants to be determined. Similarly, the following form is sought for the displacement function Φ

$$\Phi = \sum_{n=0}^{\infty} C_n \, e^{\mu_n \eta} S_n(\theta, \varphi) \tag{36}$$

Substitution of (36) into (26) yields the following characteristic equation for μ_n

$$(\mu_n^2 + \mu_n)^2 + 2P_n(\mu_n^2 + \mu_n) + Q_n = 0 \tag{37}$$

where

$$P_n = D - n(n+1)\frac{M}{2}, \quad Q_n = (n+2)(n-1)[2L + n(n+1)N] \tag{38}$$

The four characteristic roots for (37) can be solved analytically as

$$u_{n1} = \frac{-1+\sqrt{\varsigma_n}}{2}, \quad \mu_{n2} = \frac{-1+\sqrt{\xi_n}}{2}, \quad \mu_{n3} = \frac{-1-\sqrt{\varsigma_n}}{2}, \quad \mu_{n4} = \frac{-1-\sqrt{\xi_n}}{2} \tag{39}$$

where

$$\varsigma_n = 1 - 4[P_n + \sqrt{(P_n^2 - Q_n)}], \quad \xi_n = 1 - 4[P_n - \sqrt{(P_n^2 - Q_n)}] \tag{40}$$

The second subscript i ($i = 1, 2, 3, 4$) of μ_{ni} in (39) indicates the root number. When the roots for μ_{ni} are distinct, the general solution form for Φ becomes

$$\Phi = \sum_{n=0}^{\infty} (C_{n1} \, e^{\mu_{n1}\eta} + C_{n2} \, e^{\mu_{n2}\eta} + C_{n3} \, e^{\mu_{n3}\eta} + C_{n4} \, e^{\mu_{n4}\eta}) S_n(\theta, \varphi) \tag{41}$$

where C_{n1}, C_{n2}, C_{n3} and C_{n4} are constants to be determined by the boundary conditions of the sphere. Since the exact forms for Z and Φ depend on the types of the characteristic roots for μ_n and λ_n, it is necessary to discuss the possible root types for them.

5. Characteristic roots for solid spheres

Physically, all components of displacement, strain and stress must be real, therefore the displacement functions Z and Φ must be real functions of the coordinate r, θ and φ. For problems involving solid spheres, it is necessary to ensure that all stress components remain bounded as the origin is approached. Substitution of (35) and (41) into (29), (4) and (2) leads to the stress field inside the sphere, which is found to be proportional to the power $\mathrm{Re}\,[\mu_{ni}] - 1$ ($i = 1, 2, 3, 4$) and $\mathrm{Re}\,[\lambda_{ni}] - 1$ ($i = 1, 2$) of r, where $\mathrm{Re}\,[\,]$ means the real part of [ ]. Since all stress components have to be finite at $r = 0$, all r terms with power $\mathrm{Re}\,[\mu_{ni}] < 1$ or power $\mathrm{Re}\,[\lambda_{ni}] < 1$ should be discarded in view of this condition of boundedness.

It can be shown that the three characteristic roots: μ_{ni}, $i = 3, 4$ and λ_{n2} will lead to unbounded conditions at the origin of the sphere, regardless of the value of n and the elastic properties. That is,

$$\mathrm{Re}\,[\lambda_{n2}] < 1, \quad \mathrm{Re}\,[\mu_{n3}] < 1, \quad \mathrm{Re}\,[\mu_{n4}] < 1 \tag{42}$$

To see the validity of the first of (42), it can be noted that if $1 + 4M_n > 0$, λ_{n2} is real and the real

part of λ_{n2} is always less than $-1/2$ (i.e. $\mathrm{Re}\,[\lambda_{n2}] < 1$); if $1+4M_n \leqslant 0$, the real part equal exactly $-1/2$ (i.e. $\mathrm{Re}\,[\lambda_{n2}] < 1$). Consequently, we have $\mathrm{Re}\,[\lambda_{n2}] < 1$ independent of the value of n. For the validity of the second and third of (42), the following argument can be applied. If $P_n^2 - Q_n \geqslant 0$, we have three possible scenarios: for ς_n and $\xi_n \geqslant 0$, both μ_{n3} and μ_{n4} are real and the real parts of them are always less than or equal to $-1/2$; for ς_n and $\xi_n < 0$, both μ_{n3} and μ_{n4} are complex and the real parts of them equal $-1/2$; and, finally, for $\varsigma_n < 0$ and $\xi_n > 0$, μ_{n3} is complex with the real part equal to $-1/2$ and μ_{n4} is real and less than $-1/2$. If $P_n^2 - Q_n < 0$, we can let $\xi_n = A\,\mathrm{e}^{\mathrm{i}\theta}$ with the imaginary part of ξ_n being $4\sqrt{|P_n^2 - Q_n|}$, which is always positive. This implies that $0 < \theta < \pi$. Thus, $\xi_n^{1/2}$ becomes $A^{1/2}\mathrm{e}^{i\theta/2}$ with $0 < \theta/2 < \pi/2$; hence, we must have $\mathrm{Re}\,[\xi_n^{1/2}] > 0$. Consequently, if $P_n^2 - Q_n < 0$, we have $\mathrm{Re}\,[\mu_{n3}] < 1$ as shown in (39). Since for $P_n^2 - Q_n < 0$, ς_n and ξ_n are complex conjugates, so $\mathrm{Re}\,[\varsigma_n^{1/2}] = \mathrm{Re}\,[\xi_n^{1/2}] > 0$, hence $\mathrm{Re}\,[\mu_{n4}] < -1/2$. Therefore, the proof for the validity of (42) is demonstrated. Thus, to ensure the stress field to be finite at $r = 0$, we have to set the constants for all terms corresponding to λ_{n2}, μ_{n3} and μ_{n4} to zero.

The solution forms for Φ and Z now depend on the types of the possible roots for the remaining characteristic values λ_{n1}, μ_{n1} and μ_{n2}. We further note here that our problem is axisymmetric with respect to the angle φ. Thus, the spherical harmonics reduces to

$$S_n(\theta, \varphi) = P_n(\cos\theta) \tag{43}$$

where $P_n(\cos\theta)$ is the Legendre Polynomials (e.g. Abramowitz and Stegun, 1965). Therefore, all derivatives with respect to φ must be zero; consequently, it can be shown that the displacement Z is identically zero. To see this, we first express, by using (1), (4) and (29), the shear stress $\sigma_{r\varphi}$ as

$$\sigma_{r\varphi} = G' \left\{ \frac{\partial^2 Z}{\partial r\,\partial\theta} - \frac{1}{r}\frac{\partial Z}{\partial\theta} \right\} \tag{44}$$

Since only one characteristic root remains for Z (i.e. λ_{n1}), the boundary conditions (10) require that $Z \equiv 0$.

For the possible solution forms for Φ, there are six possible scenarios for the types of roots for μ_{n1} and μ_{n2}: (I) when $P_n^2 - Q_n > 0$, $\varsigma_n > 0$, $\xi_n > 0$, μ_{n1} and μ_{n2} are real unequal roots; (II) when $P_n^2 - Q_n < 0$, μ_{n1} and μ_{n2} are complex conjugates; (III) when $P_n^2 - Q_n > 0$, $\varsigma_n < 0$, $\xi_n > 0$, μ_{n1} is complex and μ_{n2} is real; (IV) when $P_n^2 - Q_n > 0$, $\varsigma_n < 0$, $\xi_n < 0$, μ_{n1} and μ_{n2} are complex but not conjugates (V) when $P_n^2 - Q_n = 0$, $\varsigma_n = \xi_n > 0$, $\mu_{n1} = \mu_{n2}$ are real (double real roots); and (VI) when $P_n^2 - Q_n = 0$, $\varsigma_n = \xi_n < 0$, $\mu_{n1} = \mu_{n2}$ are complex (double complex roots). However, for Case (III) it is straightforward to see that $\mathrm{Re}\,[\mu_{n1}] = -1/2 < 1$, thus the corresponding stress does not converge at $r = 0$. Consequently, this possible scenario is ruled out. Similarly, the solution form for Case (IV) can also be ruled out as it can show that $\mathrm{Re}\,[\mu_{n1}] = \mathrm{Re}\,[\mu_{n2}] = -1/2 < 1$. For Case (VI), it can be shown that $\mathrm{Re}\,[\mu_{n1}] = \mathrm{Re}[\mu_{n2}] = -1/2 < 1$, thus this possibility is again ruled out. For Cases (V), it is required that $P_n^2 - Q_n = 0$, which is unlikely to be satisfied by most real materials for any particular n. Therefore, these possibilities will not be considered in this study. The solutions for the remaining two possible scenarios are:

5.1. Case I: Two real roots

For any spherically isotropic material with a fixed value of n, if we find that $P_n^2 - Q_n > 0$, $\varsigma_n > 0$, $\xi_n > 0$, then μ_{n1} and μ_{n2} are real unequal roots. If μ_{n1} and $\mu_{n2} \geqslant 1$, the corresponding solution is:

$$\Phi_n = (C_{n1}\,e^{\mu_{n1}\eta} + C_{n2}\,e^{\mu_{n2}\eta})P_n(\cos\theta) \tag{45}$$

where C_{n1} and C_{n2} are real constants. If μ_{n1} and $\mu_{n2} < 1$, no converging solution can be found for solid spheres.

5.2. Case II: Two complex conjugate roots

For a particular spherically isotropic material with a specific n, if $P_n^2 - Q_n < 0$, μ_{n1} and μ_{n2} are complex conjugates. If $\mathrm{Re}\,[\mu_{n1}]$ and $\mathrm{Re}\,[\mu_{n2}] \geqslant 1$, the corresponding solution is:

$$\Phi_n = (D_n\,e^{\mu_n\eta} + \bar{D}_n\,e^{\bar{\mu}_n\eta})P_n(\cos\theta) \tag{46}$$

where $D_n = R_n + iI_n$ is a complex constant and the superimposed bar denotes the complex conjugate and μ_n becomes

$$\mu_n = \frac{-1+\sqrt{1-4P_n - i4\sqrt{|P_n^2 - Q_n|}}}{2} = x_n + iy_n. \tag{47}$$

Therefore, the general solution for Φ can now be expressed as:

$$\Phi = \sum_{n=0}^{\infty} \Phi_n \tag{48}$$

where Φ_n is defined in either (45) or (46), depending on the type of roots for μ_n.

6. The method of solutions

6.1. The general solutions of stresses

Substitution of the displacement potential into (29), (4) and (2) yields the following expressions for the stress components:

$$\begin{aligned}
\sigma_{\theta\theta} = & -\frac{1}{R}\sum_m \sum_{i=1}^{2} C_{mi}\rho^{\mu_{mi}-1}\left\{[A_{12}m(m+1)\Gamma_{mi} + (A_{13}\mu_{mi} + 2A_{12} + 2A_{66})\Lambda_{mi}]\right. \\
& \left. \times P_m(\cos\theta) - 2A_{66}\Gamma_{mi}\frac{\partial^2 P_m(\cos\theta)}{\partial\theta^2}\right\} \\
& + \frac{1}{R}\sum_n \rho^{x_n-1}\left\{P_n(\cos\theta)[\Omega_1(R_n, I_n)\cos(y_n\ln\rho) + \Omega_1(-I_n, R_n)\sin(y_n\ln\rho)]\right. \\
& \left. - \frac{\partial^2 P_n(\cos\theta)}{\partial\theta^2}[\Omega_2(R_n, I_n)\cos(y_n\ln\rho) + \Omega_2(-I_n, R_n)\sin(y_n\ln\rho)]\right\} \qquad (49) \\
\sigma_{r\theta} = & -\frac{1}{R}\sum_m \sum_{i=1}^{2}\left\{A_{44}C_{mi}\rho^{\mu_{mi}-1}[(1-\mu_{mi})\Gamma_{mi} + \Lambda_{mi}]\frac{\partial P_n(\cos\theta)}{\partial\theta}\right\}
\end{aligned}$$

$$+\frac{1}{R}\sum_n \rho^{x_n-1}[\Pi(R_n, I_n)\cos(y_n \ln\rho)+\Pi(-I_n, R_n)\sin(y_n \ln\rho)]\frac{\partial P_n(\cos\theta)}{\partial\theta} \quad (50)$$

where $\rho = r/R$ as the normalized radial coordinate. Note that the first summation for m is done over all Case I (i.e. two real roots for μ_n) while the second summation for n is done over all Case II (i.e. two complex conjugates for μ_n). The following functions have been used in these expressions:

$$\Gamma_{mi} = \Gamma_{mi}(\mu_{mi}) = d\mu_{mi}+2(a+b) \quad (51)$$

$$\Lambda_{mi} = \Gamma_{mi}(\mu_{mi}) = h\mu_{mi}(\mu_{mi}+1)-2b-am(m+1) \quad (52)$$

$$\begin{aligned}\Omega_{\mathrm{I}}(R_n, I_n) = {} & 4A_{44}(A_{12}+A_{66})[I_n(2x_n+1)y_n - R_n(x_n^2-y_n^2+x_n)] \\ & + A_{12}n(n+1)[2d(I_n y_n - x_n R_n)-4(a+b)R_n] \\ & + 2A_{44}A_{13}[(x_n I_n + y_n R_n)(2x_n+1)y_n - (x_n R_n - y_n I_n)(x_n^2-y_n^2+x_n)] \\ & + 2[2b+an(n+1)][2(A_{12}+A_{66})R_n + A_{13}(x_n R_n - I_n y_n)]\end{aligned} \quad (53)$$

$$\Omega_2(R_n, I_n) = 2A_{66}[2d(I_n y_n - x_n R_n)-4(a+b)R_n] \quad (54)$$

$$\begin{aligned}\Pi(R_n, I_n) = {} & A_{44}\{I_n y_n[2d(1-2x_n)-4(a+b)]+R_n[2d(x_n^2-y_n^2-x_n)+4(a+b)(x_n-1)]\} \\ & -2A_{44}^2[R_n(x_n^2-y_n^2+x_n)-I_n(2x_n+1)y_n]+2A_{44}[2b+an(n+1)]R_n\end{aligned} \quad (55)$$

The expression for σ_{rr} can be obtained from (49) by replacing A_{12}, $(2A_{66})$, and A_{13} by A_{13}, 0 and A_{33}, respectively; while the expression for $\sigma_{\varphi\varphi}$ can be obtained from (49) by replacing A_{12} and $2A_{66}$ by $(2A_{66}+A_{12})$ and $(-2A_{66})$, respectively.

6.2. Determination of unknown coefficients

In order to determine the unknown coefficients in these expressions, the Fourier–Legendre expansion (e.g. see Brown and Churchill, 1993) adopted by Hiramatsu and Oka (1966) is employed here to rewrite (9) as

$$\sigma_{rr} = (\cos\theta_0 - 1)p + \sum_{n=1}^{\infty} E_{2n}P_{2n}(\cos\theta) \quad (56)$$

where

$$E_{2n} = \frac{4n+1}{2n+1}[\cos\theta_0 P_{2n}(\cos\theta_0) - P_{2n-1}(\cos\theta_0)]p \quad (57)$$

The coefficients for this Fourier–Legendre expansion of the applied normal stress can be used to match with those from the internal stress field when the boundary values are considered.

By combining the shear traction free condition given in the second of (10) and (50), the following relations between C_{m1} and C_{m2} and between I_n and R_n are established:

$$C_{m1} = L_m C_{m2}, \quad I_n = K_n R_n \quad (58)$$

where

$$L_m = -\frac{(1-\mu_{m2})\Gamma_{m2}+\Lambda_{m2}}{(1-\mu_{m1})\Gamma_{m1}+\Lambda_{m1}}, \quad K_n = \frac{\Pi(1,0)}{\Pi(0,-1)} \tag{59}$$

Since σ_{rr}, $\sigma_{\theta\theta}$ and $\sigma_{\varphi\varphi}$ are even functions of θ while $\sigma_{r\theta}$ is the odd function of θ, we can replace 'n' by '$2n$' and 'm' by '$2m$' in all of the above expressions. The expression of σ_{rr} on $r = R$ must match with (56) and leads to the following solutions for $C_{2m,2}$ and R_{2n} (note that to avoid confusion the subscript $2m$ and 2 are separated by a 'comma'):

$$C_{2m,2} = -\frac{E_{2m}R}{J_{2m}}, \quad R_{2n} = \frac{E_{2n}R}{H_{2n}} \tag{60}$$

where R is again the radius of the sphere

$$\begin{aligned} J_{2m} = {} & L_{2m}[2A_{13}m(2m+1)\Gamma_{2m,1} + (2A_{13}+A_{33}\mu_{2m,1})\Lambda_{2m,1}] \\ & + 2A_{13}m(2m+1)\Gamma_{2m,2} + (2A_{13}+A_{33}\mu_{2m,2})\Lambda_{2m,2} \end{aligned} \tag{61}$$

$$\begin{aligned} H_{2n} = {} & 4A_{44}A_{13}[K_{2n}(2x_{2n}+1)y_{2n} - (x_{2n}^2 - y_{2n}^2 + x_{2n})] \\ & + 2A_{13}n(2n+1)[2d(K_{2n}y_{2n} - x_{2n}) - 4(a+b)] \\ & + 2A_{44}A_{33}[(x_{2n}K_{2n}+y_{2n})(2x_{2n}+1)y_{2n} - (x_{2n}-y_{2n}K_{2n})(x_{2n}^2 - y_{2n}^2 + x_{2n})] \\ & + 4[b+an(2n+1)][2A_{13}+A_{33}(x_{2n}-K_{2n}y_{2n})] \end{aligned} \tag{62}$$

6.3. Final solutions for stresses

By now, all unknown constants have been obtained, and substitution of (58) and (60) into (49) and (50) yields the final expressions of the stress components as

$$\begin{aligned} \sigma_{\theta\theta} = {} & \sum_m \Bigg\{ [L_{2m}\rho^{\mu_{2m,1}-1}[2A_{12}m(2m+1)\Gamma_{2m,1} + (A_{13}\mu_{2m,1} + 2A_{12} + 2A_{66})\Lambda_{2m,1}] \\ & + [2A_{12}m(2m+1)\Gamma_{2m,2} + (A_{13}\mu_{2m,2} + 2A_{12} + 2A_{66})\Lambda_{2m,2}]\rho^{\mu_{2m,2}-1}]P_{2m}(\cos\theta) \\ & - 2A_{66}[\rho^{\mu_{2m,1}-1}\Gamma_{2m,1}L_{2m} + \rho^{\mu_{2m,2}-1}\Gamma_{2m,2}]\frac{\partial^2 P_{2m}(\cos\theta)}{\partial\theta^2}\Bigg\} \times \frac{E_{2m}}{J_{2m}} \\ & + \sum_n \rho^{x_{2n}-1}\Bigg\{ P_{2n}(\cos\theta)[\Omega_1(1,K_{2n})\cos(y_{2n}\ln\rho) + \Omega_1(-K_{2n},1)\sin(y_{2n}\ln\rho)] \\ & - \frac{\partial^2 P_{2n}(\cos\theta)}{\partial\theta^2}[\Omega_2(1,K_{2n})\cos(y_{2n}\ln\rho) + \Omega_2(-K_{2n},1)\sin(y_{2n}\ln\rho)]\Bigg\} \times \frac{E_{2n}}{H_{2n}} \end{aligned} \tag{63}$$

$$\begin{aligned} \sigma_{r\theta} = {} & \sum_m \{A_{44}L_{2m}\rho^{\mu_{2m,1}-1}[(1-\mu_{2m,1})\Gamma_{2m,1} + \Lambda_{2m,1}] \\ & + A_{44}\rho^{\mu_{2m,2}-1}[(1-\mu_{2m,2})\Gamma_{2m,2} + \Lambda_{2m,2}]\} \frac{\partial P_{2m}(\cos\theta)}{\partial\theta} \times \frac{E_{2m}}{J_{2m}} \end{aligned}$$

$$+\sum_n \rho^{x_{2n}-1}[\Pi(1,K_{2n})\cos(y_{2n}\ln\rho)+\Pi(-K_{2n},1)\sin(y_{2n}\ln\rho)]\frac{\partial P_{2n}(\cos\theta)}{\partial\theta}\times\frac{E_{2n}}{H_{2n}} \quad (64)$$

and other shear stresses are zero (i.e. $\sigma_{r\varphi}=\sigma_{\theta\varphi}=0$). As mentioned previously, the expression for σ_{rr} can be obtained from (63) by replacing 'A_{12}, $(2A_{66})$, A_{13}' by 'A_{13}, 0, A_{33}', respectively; while those for $\sigma_{\varphi\varphi}$ can be obtained from (63) by replacing 'A_{12}, $(2A_{66})$' by '$(2A_{66}+A_{12})$, $(-2A_{66})$', respectively.

In the isotropic case, the coefficients in the generalized Hooke's law take the values

$$E'=E,\quad \bar{v}=v'=v,\quad G'=\frac{E}{2(1+v)} \quad (65)$$

Substitution of (65) into (63) and (64), the present solution reduces to the analytic solution by Hiramatsu and Oka (1966) for isotropic spheres subject to a pair of diametrical pointed loads, which has been found providing the theoretical basis in studying PLST for isotropic rock cores and lumps.

7. Numerical results and discussion

7.1. Stresses in isotropic spheres and comparisons with experiments

Hiramatsu and Oka (1966) concluded, by summing a finite number of terms in their analytic solution of infinite series, that the tensile stress induced along the axis through which the point loads are applied is fairly uniform (e.g. see Fig. 5 of their paper). However, a more careful study of Hiramatsu and Oka's (1966) solution by Wijk (1978) revealed that the maximum tensile stress may rise to double of the 'plateau' value in the central part of the specimen for $v=1/3$ and the tensile stress distribution is not uniform (see Fig. 3 of Wijk, 1978). This observation provides a means to check the accuracy of the present numerical results. In particular, the stresses for the case of isotropic spheres with $v=1/3$ and $\theta_0=3^\circ$ were calculated, and our results coincide with those given in Fig. 2 of Wijk (1978), as expected. To further investigate the finding by Wijk (1978), Fig. 4 plots the variations of the normalized radial and tangential stresses, $2\pi R^2\sigma_{rr}/F$ and $2\pi R^2\sigma_{\theta\theta}/F$, vs the radial distance r/R along the z-axis for various values of Poisson's ratio $v(=v'=\bar{v})$ for $\theta_0=3^\circ$. By following the usual sign convention of continuum mechanics, tension is plotted as positive. For small Poisson's ratio (say $v=0.1$), a 'local peak' near $r/R=0.9$ appears in the tensile stress concentration which is about ten times larger than those observed at the central part of the specimen. If the tensile strength or point load strength index (PLSI) is proportional to the maximum tensile stress within the specimen at the instant of failure, Fig. 4 indicates that the PLSI is extremely sensitive to the actual value of the Poisson's ratio of the rock. However, the tensile stress at the central 'plateau' and the radial compression is relatively insensitive to the change in Poisson's ratio.

Figure 5 illustrates the effect of the size of the contact zone, θ_0, on the magnitude of the local peak of tensile stress for $v=v'=\bar{v}=0.1$. Except for the varying θ_0, the plot is the same as those given in Fig 4. It is clear that the deviation of the maximum tension from the 'plateau' value at the central portion of the sphere increases drastically with the decrease of θ_0, especially for $\theta_0<5^\circ$.

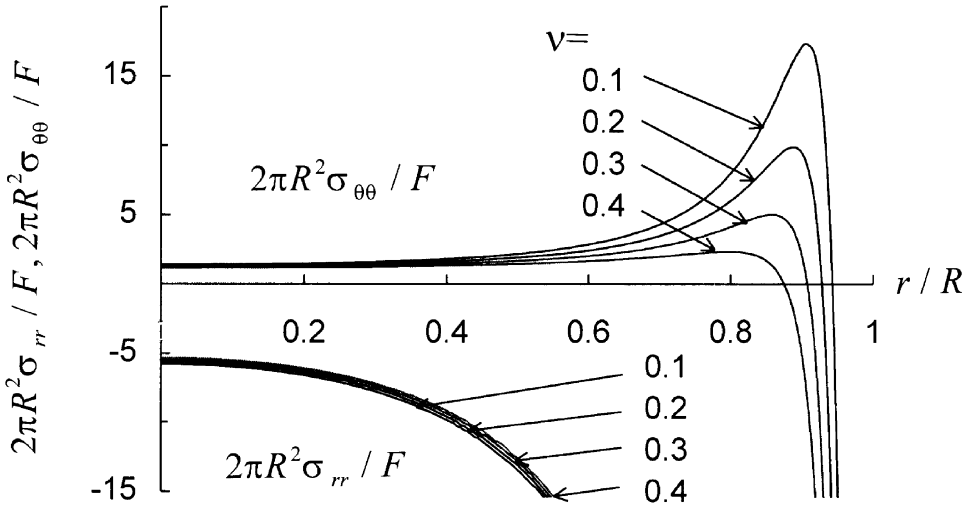

Fig. 4. Normalized stresses $2\pi R^2\sigma_{rr}/F$ and $2\pi R^2\sigma_{\theta\theta}/F$ vs the normalized radial coordinate r/R (along z-axis or with $\theta = 0^\circ$) for various values of Poisson's ratio of isotropic spheres (i.e. $\bar{\nu} = \nu' = \nu$) for $\theta_0 = 3^\circ$.

For example, the increment of the maximum tensile stress rises about 180% as θ_0 decreases from 5°–3°. For large contact zone (say $\theta_0 > 7^\circ$), the effect of the local tensile zone is not significant.

Since for the case of anisotropic spheres, there is, to the best of our knowledge, no experimental measurement on the stress concentration within a sphere under diametral point loads. Figures 6–7 compare the predictions by our solution for isotropic spheres to the experimental observations by Frocht and Guernsey (1953), as well as the theoretical prediction by Sternberg and Rosenthal (1952). More specifically, Fig. 6 plots the compressive hoop stress vs the radius r/R along $\theta = \pi/2$ for an isotropic sphere with $\nu = 0.48$ and $\theta_0 = 5^\circ$. Our prediction seems to agree better with the experiments than those by Sternberg and Rosenthal (1952), although both solutions agree well with experiments. Figure 7 plots both the radial and tangential stresses along the line between the point loads (i.e. along $\theta = 0^\circ$) for $\nu = 0.48$. Since large deformation of sphere is observed in the loaded regions in the experiment (e.g. see Fig. 8 of Frocht and Guernsey 1953), it is difficult to determine precisely the value of θ_0 in the experiments. Therefore, predictions have been obtained for both $\theta_0 = 5^\circ$ and $\theta_0 = 15^\circ$. The predictions for $\theta_0 = 15^\circ$ seems to agree better with experiments when $r/R > 0.5$, but both predictions and observations agree well for $r/R < 0.5$, independent of the values of θ_0. Thus, this plot also provides a verification of our conclusion from Fig. 5 that the tensile stresses within the central portion of the specimen (say $r/R < 0.5$) are independent of the choice of θ_0. Although there is discrepancy near the surface of the sphere, the agreement between the theoretical and experimental values is remarkably good in the neighborhood of the center of the sphere.

7.2. For anisotropic spheres

The main contribution of the present paper is in obtaining an analytic solution for spherically isotropic spheres under diametral point loads, and provides an anisotropic counterpart of the

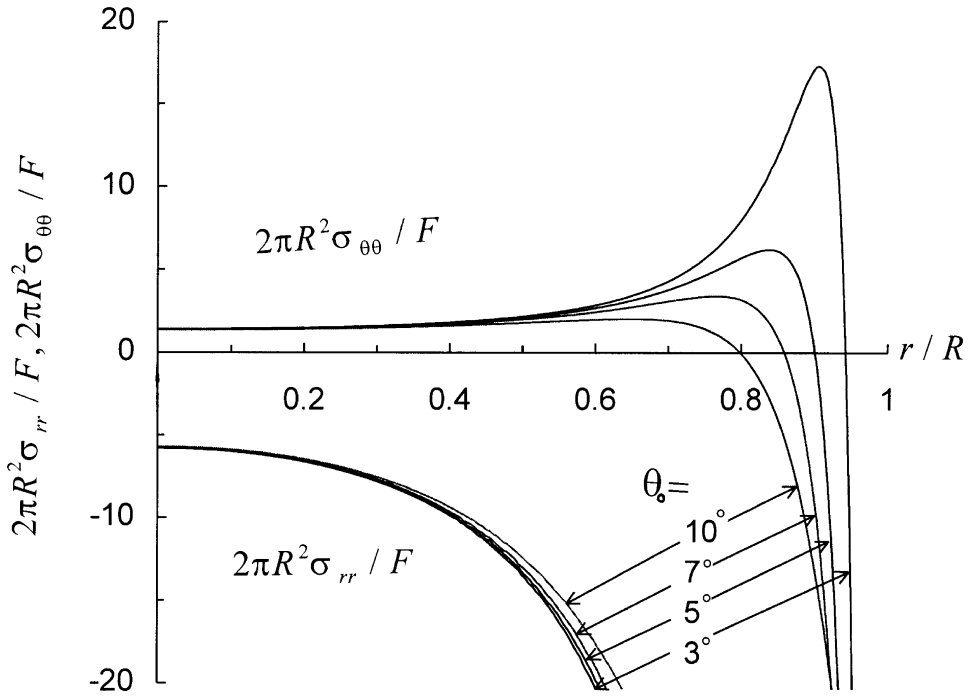

Fig. 5. Normalized stresses $2\pi R^2\sigma_{rr}/F$ and $2\pi R^2\sigma_{\theta\theta}/F$ vs the normalized radial coordinate r/R (along z-axis or with $\theta = 0^\circ$) for various values of θ_0 for isotropic spheres with $\bar{\nu} = 0.1$.

classic solution by Hiramatsu and Oka (1966) for isotropic spheres. Therefore, it is essential to investigate how the 'local tensile zone' near $r/R = 0.9$ depends on the change in the degree of anisotropy, as most rocks found in nature are anisotropic. Three parameters indicating the degree of anisotropy are defined here and will be used as the control parameters in our calculations:

$$\beta = \frac{E}{E'}, \quad \alpha = \frac{\nu'}{\bar{\nu}}, \quad \xi = \frac{A_{44}}{A_{66}} \tag{66}$$

Figure 8 plots both normalized radial and tangential stresses along the line between the center and one of the point load for various values of modulus ratio β (from 1.0–1.8) with $\alpha = \xi = 1.0$, $\bar{\nu} = 0.2$ and $\theta_0 = 3^\circ$. The maximum tensile stress at about $r/R = 0.9$ increases with β. That is, if a sphere is stiffer against axial deformation along the tangential direction than along the radial direction, it is weaker in PLST (since higher tensile stress concentration is resulted and the rock with larger β is easier to break under the same applied loads). In addition, both the radial stress and tensile stress at the center of the sphere decreases with β. Therefore, in contrast to the isotropic case, the stress concentration in anisotropic rocks is found sensitive to the value of the modulus (or the modulus ratio).

Figure 9 plots the variations of $2\pi R^2\sigma_{rr}/F$ and $2\pi R^2\sigma_{\theta\theta}/F$ vs the radial distance r/R along the z-axis for various values of $\alpha(=\nu'/\bar{\nu})$ with $\beta = 1.5$, $\xi = 1.0$, $\bar{\nu} = 0.2$ and $\theta_0 = 3^\circ$. In contrast to the effect of modulus ratio, the increase of anisotropy in terms of the changes in Poisson's ratio along

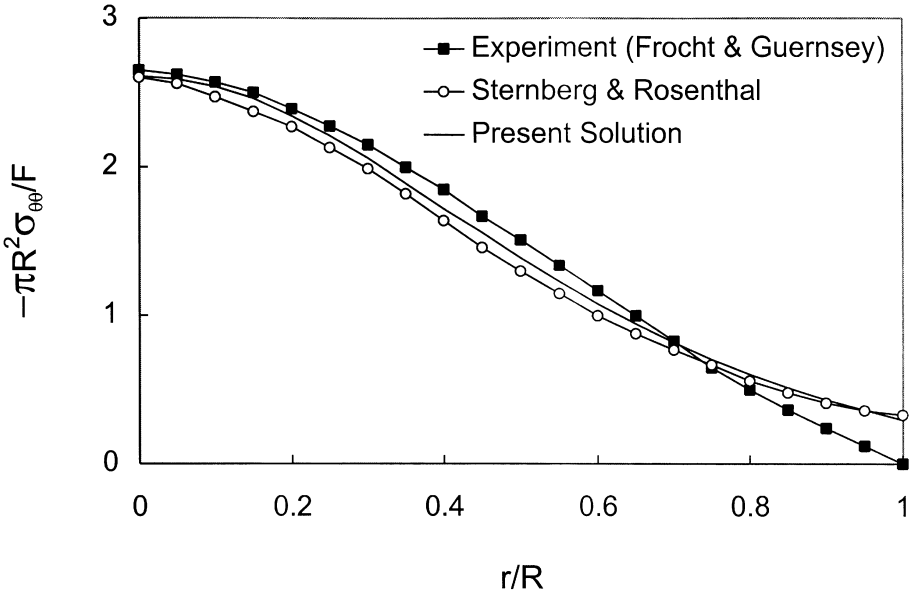

Fig. 6. The normalized tangential stress $-\pi R^2\sigma_{\theta\theta}/F$ vs the horizontal axis r/R (with $\theta = \pi/2$) for isotropic sphere with $\bar{\nu} = 0.48$. The line with squares is the experimental result by Frocht and Guernsey (1953), the line with open circles is the solution by Sternberg and Rosenthal (1952), and the solid line is our prediction for $\theta_0 = 5^\circ$.

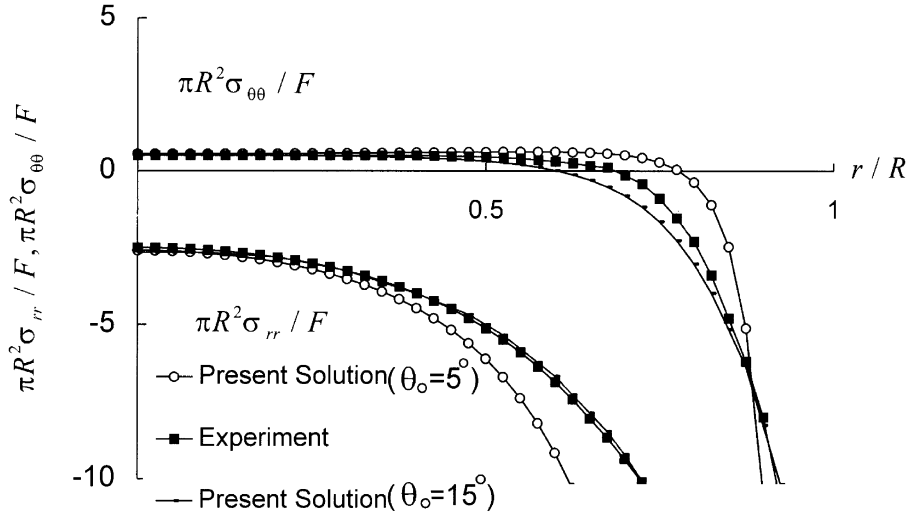

Fig. 7. Comparisons of the present solutions and the experimental results by Frocht and Guernsey (1953) for the normalized stresses $\pi R^2\sigma_{rr}/F$ and $\pi R^2\sigma_{\theta\theta}/F$ vs the normalized radial coordinate r/R (along z-axis or with $\theta = 0^\circ$) for $\bar{\nu} = \nu' = 0.48$. Our predictions for $\theta_0 = 5^\circ$ and $\theta_0 = 15^\circ$ are given in lines with circles and solid lines, respectively, while the experimental results are given in lines with squares.

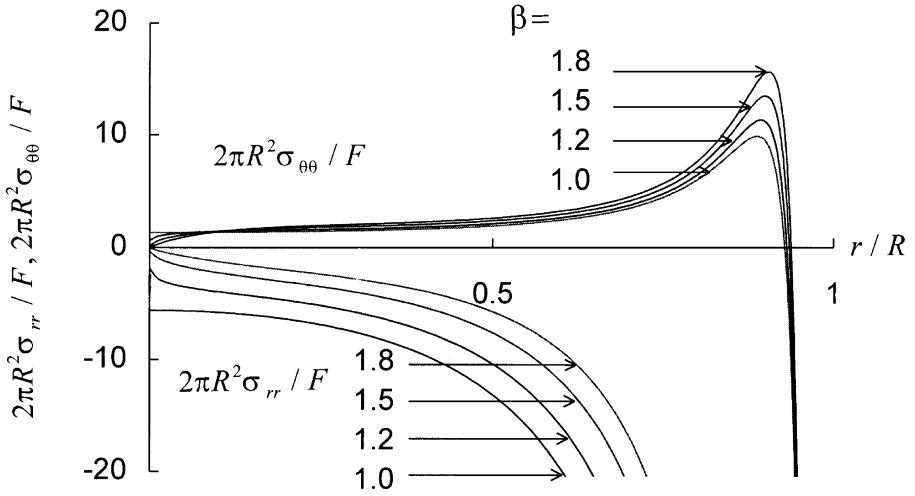

Fig. 8. Normalized stresses $2\pi R^2\sigma_{rr}/F$ and $2\pi R^2\sigma_{\theta\theta}/F$ vs the normalized radial coordinate r/R (along z-axis or with $\theta = 0^\circ$) for various values of modulus ratio β $(=E/E')$ of anisotropic spheres with $\alpha = 1.0$, $\bar{\nu} = 0.2$, $\xi = 1.0$ and $\theta_0 = 3^\circ$.

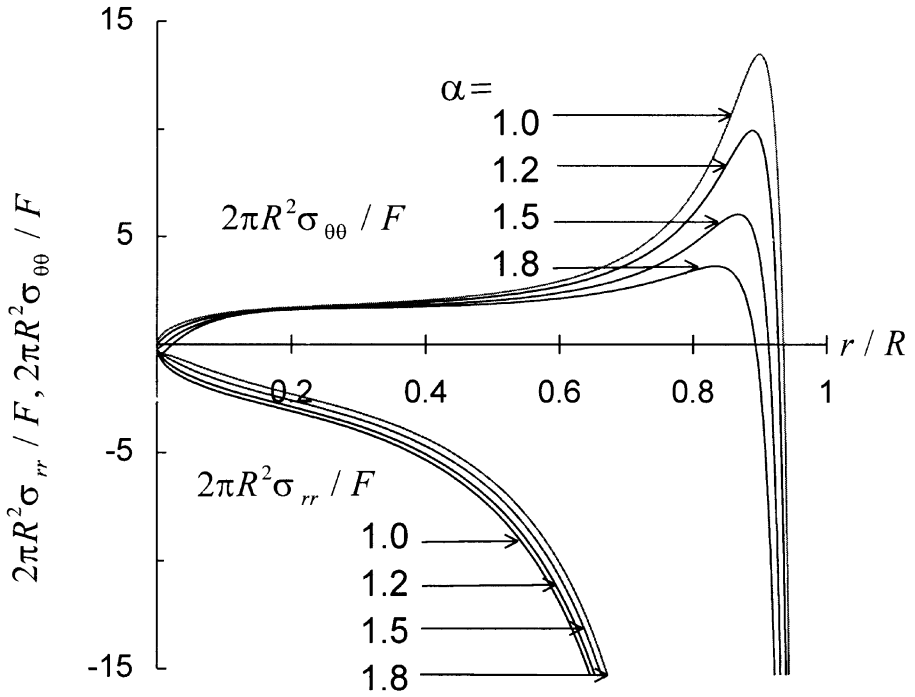

Fig. 9. Normalized stresses $2\pi R^2\sigma_{rr}/F$ and $2\pi R^2\sigma_{\theta\theta}/F$ vs the normalized radial coordinate r/R (along z-axis or with $\theta = 0^\circ$) for various values of α $(=\nu'/\bar{\nu})$ for anisotropic spheres with $\beta = 1.5$, $\nu = 0.2$, $\xi = 1.0$ and $\theta_0 = 3^\circ$.

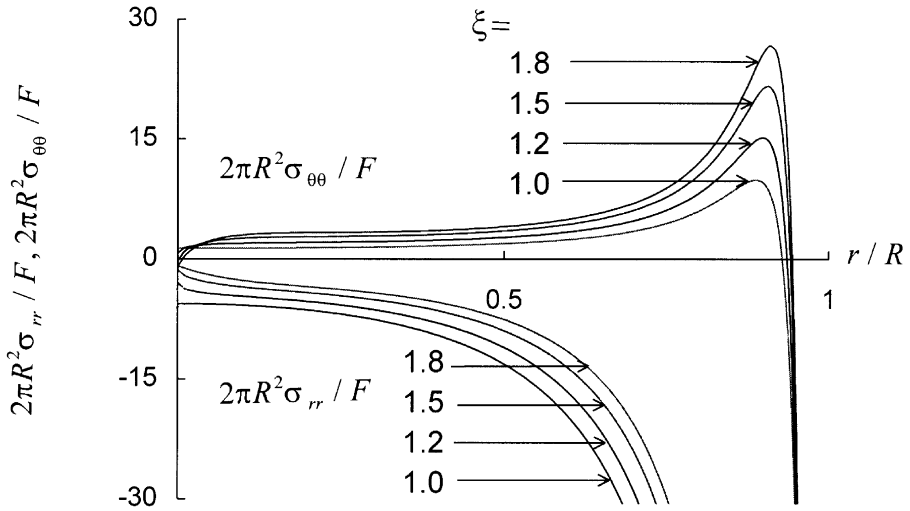

Fig. 10. Normalized stresses $2\pi R^2\sigma_{rr}/F$ and $2\pi R^2\sigma_{\theta\theta}/F$ vs the normalized radial coordinate r/R (along z-axis or with $\theta = 0^\circ$) for various values of ξ ($=A_{44}/A_{66}$) for anisotropic spheres with $\beta = 1.0$, $\bar{\nu} = 0.2$, $\alpha = 1.0$ and $\theta_0 = 3^\circ$.

different directions (i.e. increasing α) actually reduces the difference between the local tensile peak and the stress within the central part of the sphere. But, the effect of α on the radial stress is not very significant.

Figure 10 plots the normalized stresses vs r/R along the z-axis for various values of $\xi(=A_{44}/A_{66})$ with $\beta = 1.0$, $\bar{\nu} = 0.2$ and $\theta_0 = 3^\circ$. As shown in (3), A_{44} can be interpreted as the modulus governing shear deformation in the planes with normals perpendicular to the radial directions (i.e. transverse planes), and A_{66} can be interpreted as the modulus governing shear deformation in the planes of isotropy. The effect of this shear modulus ratio ξ is very similar to the observation in Fig. 8 for Young's modulus ratio β. That is, if a sphere is stiffer against shear deformation in the transverse planes than in the planes of isotropy, the local tensile stress concentration (near $r/R = 0.9$) becomes larger and, thus, it is weaker under PLST. Comparing to Fig. 8, the effect of the shear modulus ratio ξ is much larger than those of the Young's modulus ratio β. Therefore, anisotropy in shear modulus have greater effect on stress concentration than those in Young's modulus.

8. Conclusion

An analytic solution for the stress concentration inside a spherically isotropic sphere under diametral point loads is obtained by employing the 'displacement potential method' together with a Fourier–Legendre expansion for the boundary applied stress. When the isotropic limit is considered, the solution by Hiramatsu and Oka (1966) is recovered analytically. It was found that a local tensile zone near $r/R = 0.9$ is developed, and such non-uniform distribution was first pointed out by Wijk (1978) for isotropic spheres. The difference between the local maximum and the 'plateau' value in the central portion of the sphere increases with the decrease of both the Poisson's ratio and the area of the loading surface. To verify the present solution, the experimental

observations by Frocht and Guernsey (1953) for isotropic spheres with $v = 0.48$ are compared with our predictions, and the theory and experiment agree well.

For anisotropic spheres, it is found that the local maximum tensile stress increase with the degree of anisotropy in both the Young's and shear moduli, but decrease with the anisotropy in Poisson's ratio. In particular, if a sphere is stiffer against axial deformation along the tangential direction than along the radial direction, higher tensile stress concentration is observed near $r/R = 0.9$ and, thus, it is weaker in PLST. Similarly, if a sphere is stiffer against shear deformation in the transverse planes than in the planes of isotropy, the local tensile stress concentration (near $r/R = 0.9$) becomes larger and this leads to a smaller PLSI (i.e. a weaker rock). In contrast to the effect of modulus ratio, the increase of anisotropy in terms of the changes in Poisson's ratio along different directions (i.e. increasing α) actually reduces the difference between the local tensile peak and the stress within the central part of the sphere.

The present solution indicates that the tensile stress along the line of the applied point loads within the spheres is not uniform, in contrast to the conclusion by Hiramatsu and Oka (1966). The non-uniformity depends on the Poisson's ratio, size of contact zones, the degree of anisotropy of the tested rocks. In terms of further experimental verification, the local peak of the tensile zone near $r/R = 0.9$ may provide a special feature for us to assess our prediction. If experimental technique, such as the acoustic emission test, can be used to identify the origin of fracture during the point load strength test, it is possible to see whether fracture originates at about $r/R = 0.9$. Nevertheless, further experimental and theoretical studies are recommended, especially for anisotropic rocks.

Acknowledgement

This research was supported by the Research Grant Council (RGC) of the Hong Kong Government under the Earmarked Grant No. PolyU 70/96E.

Appendix

The proof for (19) given here follows that of Hu (1954). In particular, it can be shown, by eliminating either A or B from (14) and (15), that both A and B satisfy the plane Laplacian equation

$$\nabla_1^2 A = \nabla_1^2 B = 0 \tag{A1}$$

where ∇_1^2 is defined in (8). Therefore, any harmonic functions can be the solutions for A and B. However, as shown in Section V of Hu (1954), without loss of generality, both A and B can be set to zeros (i.e. $A = B = 0$). To see this, it should be first noted that the determination of u_θ and u_φ from (12) is not unique as there is a homogeneous solution for:

$$\frac{1}{r\sin\theta}\frac{\partial \psi_0}{\partial \varphi} + \frac{1}{r}\frac{\partial G_0}{\partial \theta} = 0, \quad \frac{1}{r}\frac{\partial \psi_0}{\partial \theta} - \frac{1}{r\sin\theta}\frac{\partial G_0}{\partial \varphi} = 0 \tag{A2}$$

Similar to the derivation of (A1), it is straightforward to show that both of these homogeneous solutions, ψ_0 and G_0, satisfy the plane Laplacian equation

$$\nabla_1^2\psi_0 = \nabla_1^2 G_0 = 0 \tag{A3}$$

Thus, the complete solution for ψ_0 and G_0 are harmonic functions. Alternatively, if a change of variables $\xi = \ln\tan(\theta/2)$ is introduced as suggested by Hu (1954), the solutions can be expressed in the form of complex function as $\psi_0 + iG_0 = f(\xi + i\varphi, r)$, where f is an arbitrary analytic function of the complex variable $\xi + i\varphi$. Thus, any arbitrary analytic functions ψ_0 and G_0 can be added to ψ and G without loss of generality.

Following the same procedure, one can show that the general solution for A and B given in (A1) can be written as $A + iB = F(\xi + i\varphi, r)$, where F is again any arbitrary analytic function. Without loss of generality, functions ψ_0 and G_0 can be now added to ψ and G, then the resultant u_θ and u_φ are substituted into (6). It can be shown that if the analytic function of ψ_0 and G_0 are chosen such that

$$\frac{2b}{r^2}f - h\frac{\partial^2 f}{\partial r^2} = -iF(\xi + i\varphi, r) \tag{A4}$$

then the A_0 and B_0 corresponds to ψ_0 and G_0 satisfy $A_0 + iB_0 = -F(\xi + i\varphi, r)$. Therefore, F, or in turn both A and B, can always be adjusted to zero by imposing homogeneous analytic solution f. Consequently, we can always set A and B to zero without loss of generality.

References

Abramian, B.L., Aruntiunian, H.X., Babloian, A.A., 1964. On two-contact problems for an elastic sphere. Fizika Metall. 28, 622–629 (in Russian).

Abramowitz, M., Stegun, I.A. (Eds.), 1965. Handbook of Mathematical Functions. Dover, New York.

Bieniawski, Z.T., 1974. Estimating the strength of rock materials. Journal of South Africa Institute of Mining and Metallurgy 74, 312–320.

Boisen, B.P. 1977. A hand-portable point load tester for field measurements. In: Wang, F.D., Clark, G.B. (Eds.), Energy Resources and Excavation Technology. 18th US Symposium on Rock Mechanics. Keystone, CO. pp. 5C2-1–5C2-4.

Broch, E., 1983. Estimation of strength anisotropy using the point load test. International Journal of Rock Mechanics and Mining Science 20, 181–187.

Broch, E., Franklin, J.A., 1972. The point-load strength test. International Journal of Rock Mechanics and Mining Science 9, 669–697.

Brown, J.W., Churchill, R., 1993. Fourier Series and Boundary Value Problems, 5th ed. McGraw-Hill, New York.

Chau, K.T., 1995. Bifurcation of a spherical cavity in a compressible solid with spherical isotropy. International Journal of Numerical and Analytical Methods in Geomechanics 29, 381–398.

Chau, K.T., 1998a. Analytic solutions for diametral point load strength tests. Journal of Engineering Mechanics ASCE 124, 875–883.

Chau, K.T., 1998b. Toroidal vibrations of anisotropic spheres with spherical isotropy. Journal of Applied Mechanics ASME 65, 59–65.

Chau, K.T., Wong, R.H.C., 1996. Uniaxial compressive strength and point load strength of rocks. International Journal of Rock Mechanics and Mining Science and Geomechanics Abstract 33, 183–188.

Chen, W.T., 1966. On some problems in spherically isotropic elastic materials. Journal of Applied Mechanics ASME 61, 964–970.

Chen, T.L., Durelli, A.J., 1973. Stress field in a sphere subjected to large deformation. International Journal of Solids and Structures 9, 1035–1052.
Ding, H.-J., Ren, Y.-J., 1991. Equilibrium problems of spherically isotropic bodies. Applied Mathematics and Mechanics (English edition) 12, 155–162.
Durelli, A.J., Chen, T.L., 1973. Displacement and finite-strain fields in a sphere subjected to large deformation. International Journal of Non-linear Mechanics 8, 17–30.
Durelli, A.J., Daniel, I.M., 1961. A non-destructive three-dimensional strain-analysis method. Journal of Applied Mechanics ASME Series E83, 83–86.
Eason, G., 1962. Transient thermal stresses in anisotropic bodies with spherical symmetry. Applied Scientific Research 13, 1–15.
Forster, I.R., 1983. The influence of core sample geometry on the axial point-load test. International Journal of Rock Mechanics and Mining Science 20, 291–295.
Frocht, M.M., Guernsey, J.R., 1953. A Special Investigation to Develop a General Method for Three-Dimensional Photoelastic Stress Analysis. NACA Report 1148, National Advisory Committee for Aeronautics.
Greminger, M., 1982. Experimental studies of the influence of rock anisotropy on size and shape effects in point-load testing. International Journal of Rock Mechanics and Mining Science 19, 241–246.
Guidicini, G., Nieble, C.M., Cornides, A.T., 1973. Analysis of point load test as a method for preliminary geotechnical classification of rocks. International Association of Engineering Geology 7, 37–52.
Hassani, F.P., Scoble, M.J., Whittaker, B.N., 1980. Applications of the point index test to strength determination of rock and proposals for a new size-correction chart. The State of the Art in Rock Mechanics, Proceedings of 21st U.S. Symposium on Rock Mechanics, pp. 543–553.
Hata, T., 1993. Stress-focusing effect in a uniformly heated transversely isotropic sphere. International Journal of Solids and Structures 30, 1419–1428.
Hiramatsu, Y., Oka, Y., 1966. Determination of the tensile strength of rock by a compression test of an irregular test piece. International Journal of Rock Mechanics and Mining Science 3, 89–99.
Hu, H.-C., 1954. On the general theory of elasticity for a spherical by isotropic medium. Acta Scientia Sinica 3, 247–260.
ISRM, 1985. Suggested method for determining point load strength. International Journal of Rock Mechanics and Mining Science and Geomechanics Abstract 22, 53–60.
Keer, L.M., Mowry, D.B., 1979. The stress field created by a circular sliding contact on transversely isotropic spheres. International Journal of Solids and Structures 15, 33–39.
Lajtai, E.Z., 1980. Tensile strength and its anisotropy measured by point and line-loading of sandstone. Engineering Geology 15, 163–171.
Love, A.E.H., 1944. A Treatise on the Mathematical Theory of Elasticity. Dover, New York.
Nowinski, J., (1959). Note on a thermoelastic problem for a transversely isotropic hollow sphere embedded in an elastic medium. Journal of Applied Mechanics ASME 26, 649–650.
Read, J.R.L., Thornton, P.N., Regan, W.M., 1980. A rotational approach to the point load test. Proceedings of Australia–New Zealand Geomechanics Conference, 2, pp. 35–39.
Richardson, D.N., 1989. Point-load test for estimating concrete compressive strength. ACI Materials Journal 86, 409–416.
Robins, P.J., 1980. The point-load strength test for concrete cores. Magazine of Concrete Research 32 (111), 101–111.
Robins, P.J., Austin, S.A., 1985. Core point-load test for steel-fibre-reinforced concrete. Magazine of Concrete Research 37 (133), 238–242.
Shah, K.R., Wong, T.-F., 1996. Grain fracturing and comminution in porous materials. In: Aubertin, M., Hassani, F., Mitri, H. (Eds.), Rock Mechanics, Tools and Techniques, Proceedings of 2nd North American Rock Mechanics Symposium: NARM'96. Montreal, Canada, pp. 859–866.
Shah, K.R., Wong, T.-F., 1997. Fracturing at contact surfaces subjected to normal and tangential loads. International Journal of Rock Mechanics and Mining Science 34, 727–739.
Sternberg, E., Rosenthal, F., 1952. The elastic sphere under concentrated loads. Journal of Applied Mechanics ASME 19, 413–421.
Tatara, Y., 1991. On compression of rubber elastic sphere over a large range of displacements—Part 1: Theoretical study. Journal of Engineering Materials and Technology ASME 113, 285–291.

Tatara, Y., Shima, S., Lucero, J.C., 1991. On compression of rubber elastic sphere over a large range of displacements—Part 2: Comparison of theory and experiment. Journal of Engineering Materials and Technology ASME 113, 292–295.

Wijk, G., 1978. Some new theoretical aspects of indirect measurements of the tensile strength of rocks. International Journal of Rock Mechanics and Mining Science and Geomechanics Abstract 15, 149–160.

Wijk, G., 1980. Point load test for the tensile strength of rocks. Geotechnical Testing Journal 3, 49–54.

Zhang, J., Wong, T.F., Davis, D.M., 1990. Micromechanics of pressure-induced grain crushing in porous rocks. Journal of Geophysical Research 95, 341–352.